



A Three-dimensional Plasmonic Nanostructure With Extraordinary Optical Transmission

Mohamadreza Najiminaini,^{1,2} Fartash Vasefi,^{1,2,3} Bozena Kaminska,¹ Jeffrey J.L. Carson^{2,3,*}

¹The School of Engineering Science, Simon Fraser University, Burnaby, BC, Canada

²Imaging Program, Lawson Health Research Institute, London, ON, Canada

³Medical Biophysics, Schulich School of Medicine and Dentistry, Western University, London, ON, Canada

Introduction:

The extraordinary optical transmission (EOT) of light through an array of periodic holes in metal films has been of great interest to researchers working in the areas of nano-optics and plasmonic applications [1] [2]. In contrast to standard aperture theory, at the resonances of a nano-hole array (NHA) the light transmission efficiency can exceed 100% when compared to the light incident on the nano-holes (EOT). Recent research on quasi-3D and 3D nanostructures has revealed that these devices have unique and advantageous optical properties over planar NHA structures [3]-[11]. As a result, enhancements in surface plasmon resonance (SPR) sensing and Surface Enhanced Raman Spectroscopy (SERS) for the detection of analytes were achieved by exploitation of quasi-3D nanostructures [4], [7]-[11].

Inspired by the previous studies on quasi-3D and 3D nanostructures, we developed a novel 3D nanostructure and fabrication process, which offers greater control on the nano-cavity depth with complete separation between the nano-hole and the nano-disk. The fabrication process eliminated the need for additional layers such as adhesive or conductive layers that further enhanced the optical resonance properties. The 3D nanostructure displayed strong resonance transmission mediated by the LSP effect due to small nano-cavity depths and SP coupling between the nano-holes and nano-disks. We performed a series of simulations and experiments on the 3D nanostructure in order to investigate the effect of cavity depth, nano-hole diameter, and nano-disk diameter on the optical transmission properties.

Figure 1 (a) displays a schematic of the fabrication process of a 3D nanostructure that includes a free-standing

...continued on page 2.

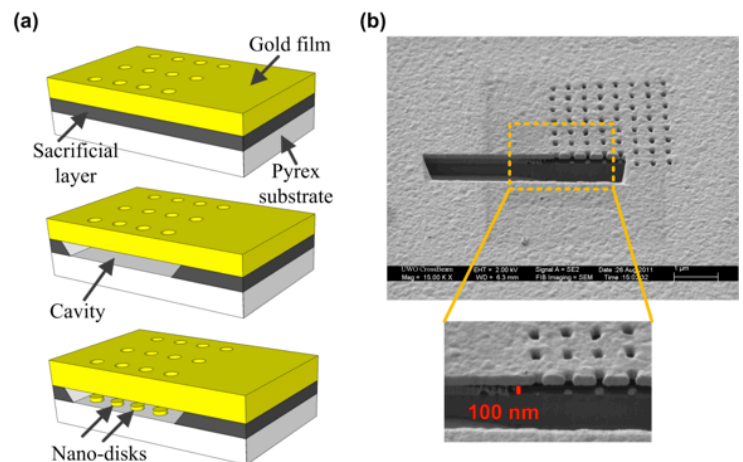
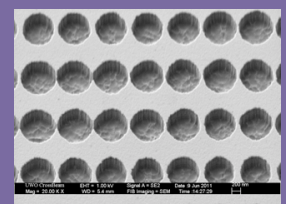
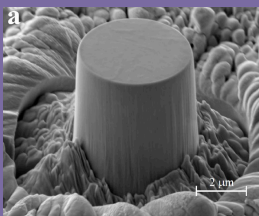


Fig. 1. a) A schematic of a NHA in a gold film fabricated on top of sacrificial and substrate layers (top), a schematic of a NHA in a gold film where the sacrificial layer has been etched to form a cavity with uniform depth beneath the NHA (middle), and a schematic of a NHA with nano-disks at the bottom of the cavity (bottom). b) SEM image (shown at an angle of 54°) of a NHA in a 100-nm gold film that was FIB milled to reveal the titanium sacrificial layer, the Pyrex substrate, and the presence of a 100-nm deep cavity that contained the nano-disks.



perforated gold film, a cavity of uniform depth, and an array of gold nano-disks at the bottom of the cavity. First, NHAs were fabricated in a 70-nm gold film on a thick Ti sacrificial layer on to Pyrex substrate using electron beam lithography (EBL; see Figure 1 (a) top) [12]. Then, a Ti etchant (TFTN, Transene company, Inc.) was used to remove the Ti sacrificial layer beneath the NHA, which resulted in a free-standing NHA gold film and a cavity underneath the NHA (see Figure 1 (a) middle). Afterwards, 30 nm of gold was deposited on to the sample using electron beam deposition, which resulted in a 30-nm thick nano-disk beneath each hole at the bottom of the cavity and increased the film thickness to 100 nm (see Figure 1 (a) bottom).

We fabricated a series of NHA devices in a free-standing 70-nm thick gold film, where the hole diameter was 100 nm, 120 nm, 140 nm, or 160 nm (circular); the periodicity was 360 nm; and the cavity depth was 100 nm or 200 nm. We then deposited 30 nm gold, which resulted in a 100-nm thick free-standing perforated film with 30-nm thick nano-disks at the bottom of the cavity located directly beneath each hole. The diameter of each nano-disk was similar to the hole diameter. Fig. 1(b) displays an SEM image of a device with a 100-nm cavity depth and 30-nm thick nano-disks at the bottom of the cavity.

In Figure 2 (a), NHAs with 100-nm and 200-nm cavity depths have a resonance transmission related to (1,0) SPP excitation from top and bottom of the perforated gold film. The same (1,0) SPP excitation occurred at both interfaces of the NHAs gold film due to the same SP energy on top and bottom of NHAs, which is a result of the same refractive index materials on both interfaces of NHAs ($n_{\text{air}}=1$). As it is illustrated in Figure 2 (b), the existence of nano-disks at the bottom of 100-nm and 200-nm cavity depths greatly affected the optical transmission spectra of NHAs. In the structure with a 100-nm cavity and nano-disks, a new resonance peak related to LSP coupling between hole and nano-disk was pronounced at 720 nm. Also, a minimum at 640 nm center wavelength for the 100-nm cavity structure resulted from absorption due to LSP interaction between hole and nano-disk. However, no resonance transmission associated to LSP coupling between hole and nano-disk was observed for the 200-nm cavity structure. This was due to the smaller SP decay length away from the metallic surface into the dielectric material for both NHA and nano-disks compared to the 200-nm cavity depth. Also, for the 200-nm cavity structure, a minimum at 650 nm wavelength was observed and was due to absorption by the nano-disks. Therefore, the optical transmission of light through the structure demonstrated optical transmission related to the product of the transmission of a NHA and an array of nano-disks.

In Figure 2 (c), as the nano-hole and nano-disk diameters increased, the LSP resonance position red-shifted for the 50 nm, 75 nm and 100 nm cavity structures. For the 100-nm cavity structure, there was agreement between the optical resonance position calculated from simulated optical spectra and the optical resonance position measured from optical

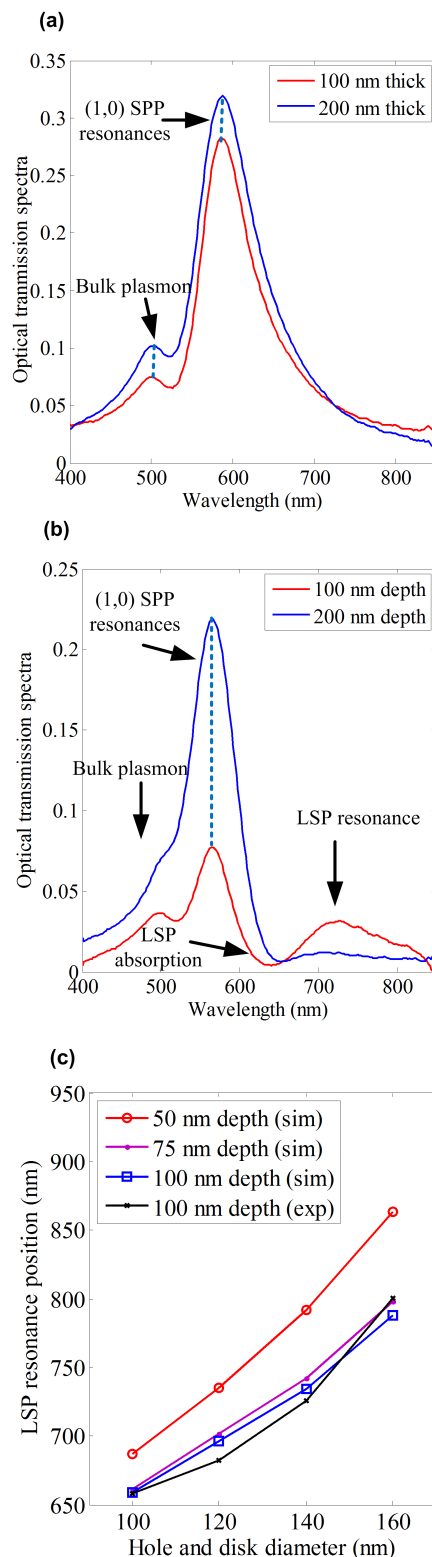


Fig. 2. a) Experimental optical transmission spectra of a 3D nanostructure with a NHA in a 100-nm thick gold film with 140 nm hole diameter and 360 nm periodicity for 100 nm and 200 nm cavity depths without nano-disks and b) with 30-nm thick nano-disks at the bottom of the cavity and c) Resonance position (LSP coupling between hole and nano-disk) of a perforated 100-nm thick gold film with 360-nm hole periodicity, 50-nm, 75 nm, and 100-nm cavity depth, and 30-nm thick nano-disks at the bottom of the cavity as a function of circular hole and nano-disk diameter taken from simulation (sim) and experimental (exp) results.

spectra collected by experiment. An estimated difference between resonance positions obtained from simulation and experiment for a given structure was between 1 nm and 14 nm. A similar red-shift occurred for the structures with 50-nm and 75-nm cavity depths for a larger hole and nano-disk size in the experimental results. Also, for the structures with 50-nm and 75-nm cavity depths, the LSP resonance position increased to a longer wavelength compared to the 100-nm cavity structure, for a given hole and nano-disk diameter. However, it was seen that the resonance peak had the largest resonance shift for the 50-nm cavity structure with respect to hole and nano-disk diameters compared to the 75-nm and 100-nm cavity depth structures. Therefore, both hole and nano-disk sizes and the distance between each hole and nano-disk influenced the LSP resonance position of the structure.

Discussion:

The fabrication process offered many benefits compared to other quasi-3D nanostructure fabrication processes. 1) The Ti layer had precise and uniform thickness and provided for a cavity of precise depth and depth uniformity compared to the photoresist spin coating process used by others [9]. 2) The glass substrate acted as an etchant stop layer to preserve cavity depth over a large area. 3) A free standing gold membrane could be achieved without the use of adhesive or conductive layers, which are known to influence and degrade the optical properties of plasmonic structures [12]. 4) The structure provided for SP energy matching between the top and bottom surface of the perforated gold film, which is recognized to enhance the optical properties. 5) The structure is amenable to deposition of liquids and gases and benefits from the same refractive index above and below the gold film, which is not possible with other quasi-3D nanostructure designs (e.g. see [4]-[11]). 6) The free standing perforated gold film (e.g. membrane) provides for complete separation between the nano-hole and the nano-disk, which is not easily achieved with other fabrication methods for small cavity depths.

References:

1. T. W. Ebbesen, H. J. Lezec, H. F. Ghaemi, T. Thio, and P. A. Wolff, "Extraordinary optical transmission through sub-wavelength hole arrays," *Nature* **391**, 667-669 (1998).
2. A. Lesuffleur, H. Im, N. C. Lindquist, K. S. Lim, and S. Oh, "Laser-illuminated nanohole arrays for multiplex plasmonic microarray sensing," *Opt. Express* **16**, 219-224 (2008).
3. J. Yang, H. Gao, J. Y. Suh, W. Zhou, M. H. Lee, and T. W. Odom, "Enhanced Optical Transmission Mediated by Localized Plasmons in Anisotropic, Three-Dimensional Nanohole Arrays," *Nano Lett.* **10**, 3173-3178 (2010).
4. M. E. Stewart, N. H. Mack, V. Malyarchuk, J. A. N. T. Soares, T. Lee, S. K. Gray, R. G. Nuzzo, and J. A. Rogers, "Quantitative multispectral biosensing and 1D imaging using quasi-3D plasmonic crystals," *PNAS* **103**, 17143-17148 (2006).
5. J. Li, S. Chen, Y. Chou, M. Wu, C. Hsueh, and W. Su, "Effects of Gold Film Morphology on Surface Plasmon Resonance Using Periodic P3HT:PMMA/Au Nanostructures on Silicon Substrate for Surface-Enhanced Raman Scattering," *J. Phys. Chem. C* **115**, 24045-24053 (2011).
6. W. Li, J. Hu, and S. Y. Chou, "Extraordinary light transmission through opaque thin metal film with subwavelength holes blocked by metal disks," *Opt. Express* **19**, 21098-21108 (2011).
7. A. Artar, A. A. Yanik, and H. Altug, "Fabry-Perot nanocavities in multilayered plasmonic crystals for enhanced biosensing," *Appl. Phys. Lett.* **95**, 051105-3 (2009).
8. J. Xu, P. Kvasnicka, M. Idso, R. W. Jordan, H. Gong, J. Homola, and Q. Yu, "Understanding the effects of dielectric medium, substrate, and depth on electric fields and SERS of quasi-3D plasmonic nanostructures," *Opt. Express* **19**, 20493-20505 (2011).
9. J. Xu, P. Guan, P. Kvasnicka, H. Gong, J. Homola, and Q. Yu, "Light Transmission and Surface-Enhanced Raman Scattering of Quasi-3D Plasmonic Nanostructure Arrays with Deep and Shallow Fabry-Perot Nanocavities," *J. Phys. Chem. C* **115**, 10996-11002 (2011).
10. F. Bezares, J. Caldwell, O. Glembocki, R. Rendell, M. Feygelson, M. Ukaegbu, R. Kasica, L. Shirey, N. Bassim, and C. Hosten, "The Role of Propagating and Localized Surface Plasmons for SERS Enhancement in Periodic Nanostructures," *Plasmonics* **7**, 143-150 (2012).
11. A. J. Baca, J. M. Montgomery, L. R. Cambrea, M. Moran, L. Johnson, J. Yacoub, and T. T. Truong, "Optimization of Nanopost Plasmonic Crystals for Surface Enhanced Raman Scattering," *J. Phys. Chem. C* **115**, 7171-7178 (2011).
12. M. Najiminaini, F. Vasefi, B. Kaminska, and J. J. L. Carson, "Optical resonance transmission properties of nano-hole arrays in a gold film: effect of adhesion layer," *Opt. Express* **19**, 26186-26197 (2011).

This newsletter is a part of the paper published in *Plasmonics*, 1-8, (2012) under the authorship of Mohamadreza Najiminaini, Fartash Vasefi, Bozena Kaminska, and Jeffery J.L. Carson. Retrieved from <http://dx.doi.org/10.1007/s11468-012-9378-9> (The original source of this publication is springerlink.com)

Dear Western Researchers,

The Western Nanofabrication Facility is pleased to support three projects to be conducted in our facility by Western Researchers. The "Nanofabrication Facility Sponsorship Award" will cover up to \$1500 of expenses (standard academic cost of nanofab usage) for projects involving graduate students who will be trained in the facility on the desired fabrication instruments. This year the three selected graduate student nominee's are:

Annemarie Pickersgill - (Prof. Gordon Osinski & Prof. Roberta Flemming, Dept. of Earth Sciences) - *An Accurate Determination of Shock Level in Feldspar Group Minerals.*

Maria Goiko - (Prof. John de Bruyn, Physics and Astronomy & Prof. Brian Heit, Microbiology and Immunology) - *Cellular Mechanisms of Force Generation in Antibody-Mediated Phagocytosis.*

Ryan Guterman - (Prof. Paul Ragona, Dept. of Chemistry) - *Photolithographic Patterning of Phosphonium Salt Polymers*

All three students are new users of the facility, with a well defined nanofabrication and/or nano characterization project. We hope to offer such awards every year. Announcements will be done over the summer.

Sincerely,
Western Nanofabrication Facility.



Pore Morphometrics and Thermal Evolution of Organic-Matter Microporosity, Colorado Group, Western Canada Sedimentary Basin

Peng Jiang, Burns Cheadle

Department of Earth Sciences, Western University, London, Ontario N6A 5B7

The broad areal extent of the WCSB and the availability of samples throughout the basin provide an excellent framework for studying organic matter micropore morphometrics in relation with thermal maturity. Imaging and pore characterization of the samples from Colorado Group of the WCSB has been conducted using the FIB/SEM system (LEO (Zeiss) 1540XB) in Western University's Nanofabrication Facility. Phyllosilicate framework porosity (PF) pores and organic matter (OM) pores are the dominant pore types in the lower Colorado Group (Fig.1). OM pores are thought to develop as a result of kerogen degradation during catagenesis, and are considered as evidence of thermal maturity of the carbonaceous mudstone (Curtis et al., 2010). However, the Colorado Group samples analyzed thus far appear to exhibit exceptions to this hypothesis. OM pores are distributed in a manner that is not readily related to thermal maturity or burial history. This contributes to a high level of reservoir heterogeneity that presents significant challenges for flow characterization. Coccoliths are common in these samples (Fig. 2). They are found as mainly individual clasts and some are aggregates. Preservation is moderate to good. As a result of abundant fecal pellets composed of coccolithic debris, the Second White Specks Formation has a speckled appearance (Bloch et al., 1993). In addition, pyrite exists in almost all the samples. The crystal form is usually octahedral, act as a single large crystals or small aggregates or pyrite framboids (Fig. 3).

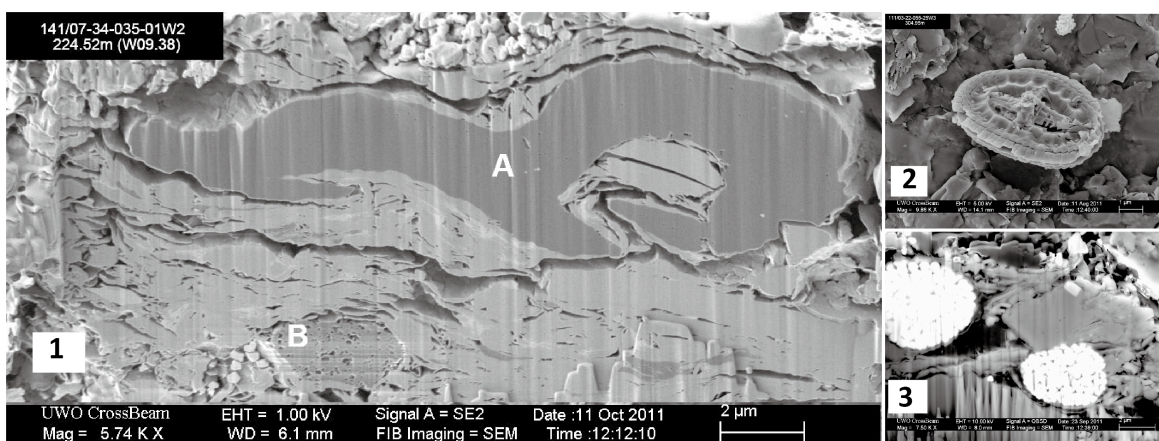


Figure (1) SEM image from 141/07-34-035-01W2 (224.52 mKB) illustrates heterogeneity of OM porosity development. Notice that OM porosity development in kerogen maceral "A" is limited to isolated micropores, whereas kerogen maceral "B" exhibits denser development of larger micro- to meso-pores. **(2)** An intact coccolith with well preserved structure. Taxonomic classification of the species has not been determined. **(3)** BSE image shows pyrite framboids as bright area.

References:

Bloch, J., Schröder-Adams, C., Leckie, D., McIntyre, D., Craig, J., and Staniland, M., 1993, Revised stratigraphy of the lower Colorado Group (Albian to Turonian), Western Canada: *Bulletin of Canadian Petroleum Geology*, v. 41, p. 325.
 Curtis, M., Ambrose, R., and Sondergeld, C., 2010, Structural Characterization of Gas Shales on the Micro- and Nano-Scales. SPE Paper 137693, Canadian Unconventional Resources and International Petroleum Conference, 19-21 October 2010, Calgary, Alberta, 15p.

Western Nanofabrication Facility

Western University
 Physics and Astronomy Building Room 14
 London, Ontario N6A 3K7

nanofab.uwo.ca



Western
 Science

Prof. François Lagugné-Labarthet
 Facility Director
 flagugne@uwo.ca

Todd Simpson Ph.D.
 Senior Research Scientist
 tsimpson.uwo.ca

Tim Goldhawk
 Laboratory Supervisor
 tim.goldhawk@uwo.ca

Dear Nanofabrication graduate students and post-docs, send us a summary of your research project that was done in the Nanofab and receive a \$100 gift card for the Western University bookstore. Your summary could be published in the next NanoWestern newsletter